

Thermomechanical Analysis of High-Heat-Load Components for the Canted-Undulator Front End

Y. Jaski, E. Trakhtenberg, J. Collins, C. Benson,
B. Brajuskovic, and P. Den Hartog

*Advanced Photon Source, Argonne National Laboratory, Argonne, IL 60439, U.S.A.
Phone: (630) 252-4661, Fax: (630) 252-9350
e-mail: jaskiy@aps.anl.gov*

Abstract

With the canted undulators operating at 200 mA at closed gap at the Advanced Photon Source in the future, the front end will receive 20.4 kW of total power and 281 kW/mrad² of peak power density. Thermal analysis of the front-end high-heat-load components becomes an essential part of the front-end design. An extensive study has been conducted on the thermal design of the photon shutters and fixed masks. A unique dog-bone-shaped cross-section design for the photon shutters was derived to relieve high stress in the corners. The dual-undulator x-ray beams were simulated at several locations on the fixed mask to ensure the worst possible case is considered. Stress analysis on the fixed mask revealed that the maximum stress occurs when beam hits the intersection between the horizontal surface and the corner surface. The details of the analysis procedure are presented, and the failure criteria are discussed.

Keywords: front end, canted undulator, fixed mask, photon shutter, high heat load

1. Introduction

In order to increase the total number of beamlines available to users, canted undulators are used, which will produce two beams with 1 mrad horizontal separation. Each undulator is 2.07 m long. The center of one undulator will be 1.25 m upstream of the center of the straight section, and the center of the other undulator will be 1.25 m downstream of the center of the straight section. The front-end thermal management components from upstream to downstream include first fixed mask (FM1), second fixed mask (FM2), first photon shutter (PS1), second photon shutter (PS2), exit splitter mask and beryllium window. The dual beams are contained within the same aperture until going through the exit splitter mask. The fixed masks are used to collimate the x-ray beams and limit beam missteering, whereas the photon shutters are used to fully intercept the beams. However, both components are designed to withstand the full x-ray beams from the canted undulators. This paper focuses on the design and analysis of the photon shutters and fixed masks.

2. Power Calculation

2.1 Undulator Parameters

The worst case, from the standpoint of total power and power density, is when the canted undulators are at closed gap with beam current of 200 mA. The undulator and storage ring parameters are listed in Table 1.

Table 1: Canted Undulator Parameters

Maximum beam current	200 mA
Length of each undulator	2.07 m
Undulator period length λ	3.3 cm
Number of periods N	62
Undulator minimum gap	10.5 mm
Corresponding deflection parameter K	2.76
Horizontal beam size σ_x	352 μm
Vertical beam size σ_y	18.4 μm
Horizontal beam divergence σ_x'	22 μrad
Vertical beam divergence σ_y'	4.2 μrad
Total power emitted from each undulator	10.2 kw
Total power emitted from dual undulators	20.4 kw
Peak power density at normal incidence	281 kw/mrad ²

2.2 Power Calculation

To perform the thermal analysis efficiently, calculating the spatial distribution of power density from the undulator at different gaps accurately and conveniently is essential. In the synchrotron community, XOP [1] is widely used for undulator power and spectrum calculations. However the power density output data from XOP is a matrix. To apply the power density results from XOP to a finite element model, curve fitting or data interpolation between the different mesh sizes in XOP and in the finite element analysis (FEA) model must be done, and this process can be time consuming. Fortunately, there is another synchrotron source calculation package available called SRUFF [2], which was developed by Dr. Mati Meron in APS CARS-CAT over the past five years. The source code of SRUFF is written in IDL and runs in IDL; SRUFF is very powerful and engineering friendly. It can calculate spatial distribution of power density of raw power, power absorbed in media, power transmitted through media, and power reflected from mirrors. The output data can be fit into an equation up to 4th-order Gaussian within SRUFF. The equation is then used in engineering analysis software such as ANSYS for thermal analysis. For raw power density calculation, SRUFF is based on the exact analytical expression of angular distribution of undulator power [3], which accounts for an infinite number of harmonics, while XOP integrates the power from the contributing finite number of harmonics. So the results from SRUFF are slightly more conservative compared to those from XOP. The difference of peak power density and total power calculated by SRUFF and by XOP is less than 1%.

To illustrate the convenience of using SRUFF, the total power and power density of PS2 is calculated. The PS2 is located 22 m from the center of the straight section. The distance from PS2 to the center of the downstream undulator is 20.75 m and to the center

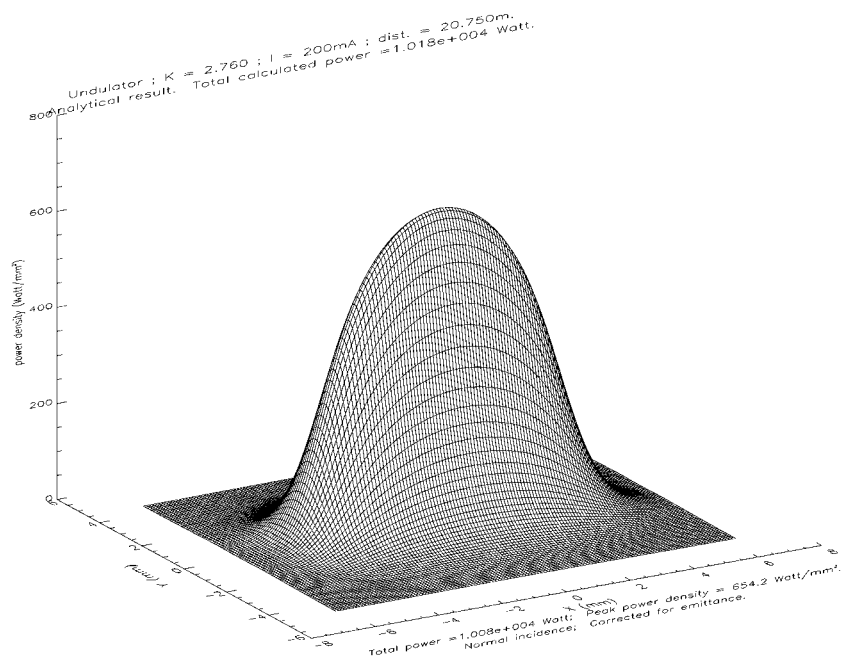


Fig. 1: Power density distribution of undulator A at 20.75 m, $k = 2.76$, $I = 200$ mA, $\lambda = 3.3$ cm, $N = 62$.

$$\text{Fit} = \exp(6.4834 - 0.024199x^2 - 0.72106y^2 - 0.0032629x^4 + 0.037042y^4 + 0.0038910x^2y^2)$$

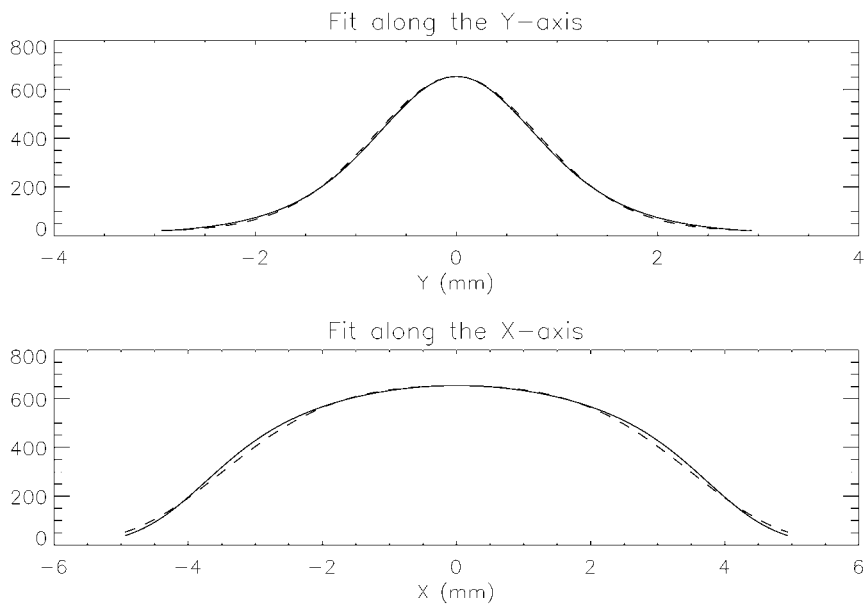


Fig. 2: Undulator power density at 20.75 m, $k = 2.76$, $I = 200$ mA. $\lambda = 3.3$ cm, $N = 62$; solid line is the exact value, and the dashed line is the fitted equation.

of the upstream undulator is 23.25 m. The power density of the downstream undulator at the PS2 location at closed gap is calculated by SRUFF and plotted in Fig. 1. The data matrix is fit into the equation shown in Fig. 2 within SRUFF. This equation will be used in the FEA model for the thermal analysis. The power density data are usually fit with a 4th-order or 2nd-order Gaussian depending on the fitting range or aperture size.

3. Design and Analysis of Photon Shutters

3.1 Design Concept Evolution

The designs of PS1 and PS2 are similar with a minor difference in apertures. The initial design concept of the shutter was a box-cone-shaped mask capable of tilting downward. At the open position, it works just like a mask with a horizontal and vertical taper angle. It can tilt downward to stop the beam with the upper surface. The incident angle to the beam at closed position is the initial mask taper angle plus the tilting angle. At the closed position, the top surface of the shutter has a vertical incident angle of 0.91° to the beam for both PS1 and PS2. Thermal and stress analyses showed high stress in the upper corners, although incident beams are at the top surface away from the corner. It was apparent that stress relief at the corner was needed. The next approach we tried was to cut a stress relieve groove in the corner from the interior surface. The stress analysis showed that the cut did not provide enough stress relief. In addition, the cut itself initiates tensile stress, so this idea was abandoned. The next approach was to cut a stress-relief groove near the corner from the exterior surface to make the mask body more flexible. This approach is very sensitive to how deep and wide the groove is. If the groove is too shallow, it does not provide enough stress relief, and, if the groove is too deep, it induces a large tensile stress. So this idea was abandoned as well. Finally, we derived the dog-bone shaped design (shown in Fig. 3) by giving up the function as a horizontal mask. The dog-bone-shaped cross section completely relieves the lateral stress at the corner resulting from corner constraints. However, the overall stress of the photon shutter is still larger than that of a simple plate because the box shape is more rigid than a plate, so the longitudinal stress is larger.

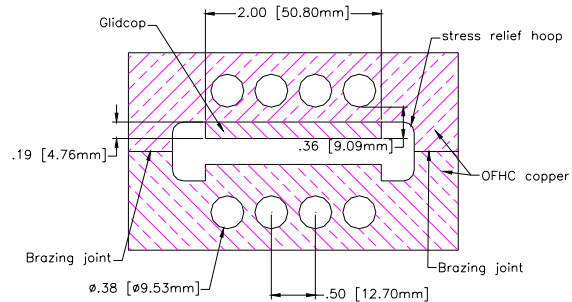


Fig. 3: PS2 dog-bone shaped cross section at mid length

3.2 Shutter Design Feature and Thermal Analysis

The PS1 and PS2 bodies are made by brazing the top and bottom halves together. The top half is made of OFHC copper with a 3/16-inch-thick Glidcop face plate brazed to it. At the closed position, the Glidcop face plate will intercept the full beam. The bottom half is made of only OFHC copper because the bottom half has a mere 0.24° incidence angle to the beam at open position for both PS1 and PS2 and will not encounter beam at the closed position. Both PS1 and PS2 have eight 3/8-inch-diameter cooling channels.

Copper wire coils are inserted into the cooling channels to obtain an enhanced convection heat transfer coefficient [4]. The thickness from the hot wall to the cooling wall was increased to 9 mm from the 6.35 mm used in the existing front-end design to lower the cooling channel temperature. The material properties used in the analysis are listed in Table 2. Thermal and stress analysis results are tabulated in Table 3 and plotted in Fig. 4 and Fig. 5.

Table 2: Material Properties of Glidcop and OFHC Copper

Thermal mechanical properties	Glidcop AL-15 flat plate up to 10 mm thick [5]	OFHC copper [6]
Thermal conductivity (w/mm°C)	0.365	0.391
Coefficient of thermal expansion (µm/m)	16.6	17.7
Young's modulus (GPa)	130	115
Poisson's ratio	0.326	0.343
Yield strength (MPa) (as consolidated – cold worked)	331 - 455	69 - 365
Tensile strength (MPa) (as consolidated – cold worked)	413 - 483	221 - 455

Table 3: Temperature and Equivalent Stress Results of PS1 and PS2
 (I=200 mA, incident angle 0.91°, h=0.015 w/mm²°C, T₀=20 °C)

Case	PS2 (k=2.76)	PS2 (k=2.62)	PS1 (k=2.76)	PS1 (k=2.62)
Peak incidental power density (w/mm ²)	10.4	9.8	12.7	12.0
T _{max} on Glidcop (°C)	248	227	278	255
T _{max} on OFHC copper (°C)	163	149	180	164
T _{wall} (°C)	129	118	143	131
σ _{eff} (MPa)	347	317	394	360

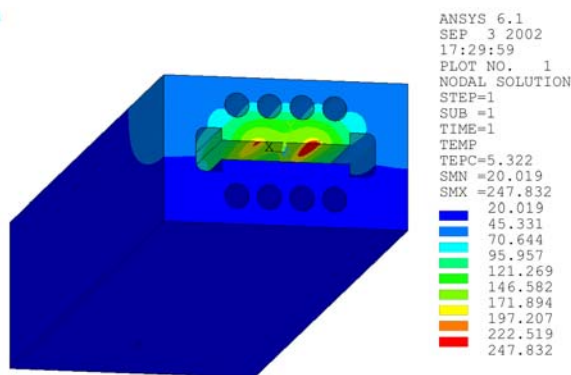


Fig. 4: PS2 temperature in °C at 200 mA, k=2.76.

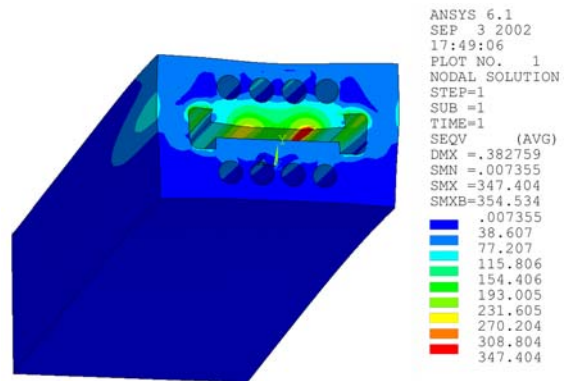


Fig. 5: PS2 equivalent stress in MPa at 200 mA, k=2.76.

The following criteria were used to determine if the design of the shutter is safe and sound.

- **Maximum cooling channel wall temperature:** The maximum cooling channel wall temperature must be kept below the water boiling temperature at the channel pressure as a precaution to prevent thermal runaway. In the shutter design, the hot-wall-to-cooling-wall distance is increased to reduce the cooling-channel wall temperature. The existing APS front-end shutter operation is limited to 130 mA beam current at closed gap because the shutter cooling channel temperature exceeds the boiling temperature of water at the higher current. Another improvement in this design is to use copper-wire coil inserts instead of copper mesh to enhance heat transfer. Because the pressure drop in a wire coil is much less than the pressure drop in the mesh, the cooling channel pressure is raised, so the saturation temperature rises. The pressure drop is about 1.3 psi/inch for 2 gpm flow rate [4]. The inlet pressure is typically above 110 psig, and the shutter length is 24 inches. This gives an outlet pressure of no less than 75 psig. The saturation temperature at 75 psig is 160°C.
- **Material strength and fatigue life:** In previous versions of the front-end design, the maximum equivalent stress limit was set at the material yield stress in the consolidated state. This is a very conservative approach because the thermal loading cycle effectively cold works the material so that the material yield stress is higher than the consolidated state. Furthermore the thermal stress is mainly a compressive stress, which does not initiate cracks. As long as the stress level stays below the low-400 MPa range, it is considered safe. The stress in the existing front-end shutters is already at 384 MPa operating at 130 mA at 11 mm gap. For fatigue consideration, the maximum temperature on the Glidcop face plate should be below 300°C, and the maximum temperature on the OFHC should be below 150°C when possible [7]. However, fatigue concerns only apply to PS2 and not PS1, because PS1 is a backup shutter and is used infrequently under abnormal conditions.

4. Thermal and Stress Analysis of Fixed Masks

Due to the space limitations in the front end, the conventional box-cone-shaped design is used. The box-cone shape is a highly constrained geometry, which induces larger stress levels than would occur in a plate. In order to handle the expected higher stress at the corner, the fixed mask body is made out of a Glidcop bar with cross-section dimensions of 4.5×3.5 inches. Thermal and stress analyses are performed with a full

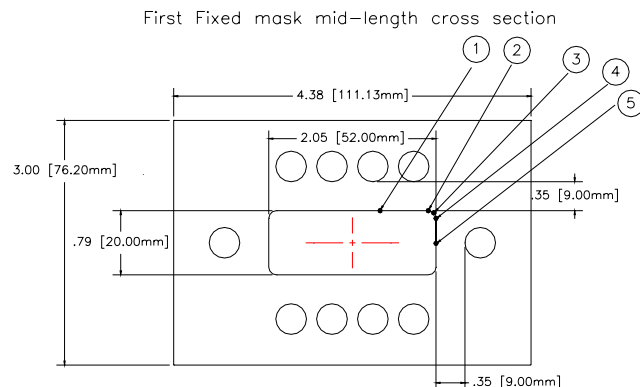


Fig. 6: Location of the center of the downstream beam for the analysis.

model because the boundary condition cannot be accurately specified by using half or a quarter model. Using only a half or a quarter model with improper boundary conditions usually leads to an underestimate of the overall stress level, especially in the corners. The analyses are performed with the downstream beam in the five locations shown in Fig. 6. The upstream beam is 1 mrad away. The apertures and power density of FM1 and FM2 are listed in Table 4 and the temperature and equivalent stress results are tabulated in Table 5 and shown in Fig. 7 and Fig. 8.

Table 4: FM1 and FM2 Apertures and Power Density

	FM1	FM2
From inlet to the center of the straight section (m)	16.9	17.7
Inlet aperture (mm)	[64 × 26]	[46 × 17]
Exit aperture (mm)	[40 × 14]	[26 × 5]
Device active length (mm)	600	600
Vertical taper angle	0.57°	0.57°
Horizontal taper angle	1.15°	0.95°
Peak vertical incidence power density (w/mm ²)	11.0	10.1
Peak horizontal incidence power density (w/mm ²)	22.2	16.8

Table 5: Thermal and Stress Results of FM1 and FM2 (I=200 mA, k=2.76, h=0.015 w/mm²°C, T₀=20 °C)

Location (see Fig. 6)	1	2	3	4	5
FM1 T _{max} (°C)	218	216	194	158	167
FM1 σ _{eff} (MPa)	353	397	335	234	255
FM2 T _{max} (°C)	198	189	167	134	133
FM2 σ _{eff} (MPa)	333	401	327	203	208

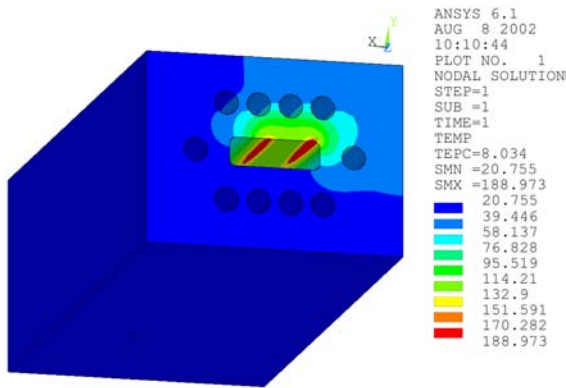


Fig. 7: FM2 temperature in °C with beam at position #2.

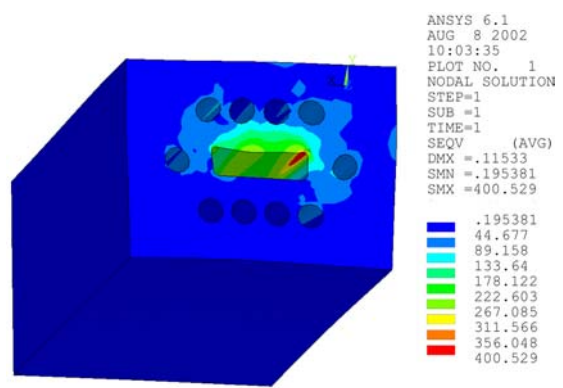


Fig. 8: FM2 equivalent stress in MPa with beam at position #2.

From Table 5 we see the temperature and stress at the beam horizontal missteering (position #5) is much lower than those of the beam vertical missteering (position #1), although the power density at horizontal missteering is higher. This is because the beam has a larger horizontal than vertical size; the beam footprint is thin and long for horizontal missteering while fat and short for vertical missteering. For a glazing-incidence high-heat-load device, the power per unit length of the beam footprint governs the heat-transfer characteristics. We also note that the highest stress occurs when beam is centered at the intersection of the corner and a horizontal surface (position #2). At this position, the corner constraint contributed greatly to the high stress, and the smaller the aperture, the greater the stress. So the stress on FM2 is larger than on FM1. When the beam is centered at position #3 or #4, the beam footprint becomes longer and both temperature and stress are decreased.

5. Summary

The photon shutters and fixed masks for the canted undulator front end are currently under fabrication. The front end for canted undulator is designed for a maximum beam current of 200 mA at closed gap.

6. Acknowledgments

The authors thank Dr. Mati Meron of CARS-CAT for providing us the synchrotron source calculation package SRUFF. The authors also thank S. Picologlou for editing this paper. This work was supported by the U.S. Department of Energy, Office of Basic Energy Sciences, under Contract No. W-31-109-ENG-38.

7. References

- [1] M. Sanchez del Rio and R. J. Dejus, "XOP: A Multiplatform Graphical User Interface for Synchrotron Radiation Spectral and Optics Calculations," SPIE Proc., vol. 3152, 148-157, 1997.
- [2] Mati Meron, "SRUFF: A Comprehensive Package for Synchrotron Radiation Spectral and Optics Calculations," unpublished.
- [3] Kwang-Je Kim, "Angular Distribution of Undulator Power For An Arbitrary Deflection Parameter K," Nucl. Instrum. Methods, A246 (1986) 67-70.
- [4] J. Collins, C. Conley, J. Attig, "Enhanced Heat Transfer Utilizing Wire-Coil Inserts for High-Heat-Load Applications," to be published in MEDSI 2002 proceedings, 2002.
- [5] "Glidcop Grade AL-15 Dispersion Strengthened Copper," Technical data, SCM Metal Products, Inc., 1988.
- [6] R. Green, "Machinery's Handbook," 24th Edition, 1992.
- [7] S. Sharma, E. Rotela and A. Barcikowski, "High Heat-Load Absorbers for the APS Storage Ring," MEDSI 2000 proceedings, 2000.